https://doi.org/10.5194/egusphere-2024-4169
Preprint. Discussion started: 17 February 2025

Effects of synoptic atmospheric variability on sub-daily precipitation $\delta^{18}O$-air temperature functions in reconstructions of pre-instrumental $\delta^{18}O$ chronicles across Europe

Guilhem Türk[1], Christoph J. Gey[2], Bernd R. Schöne[2], Laurent Pfister[1]

[1] CATchment and ecohydrology research group, Environmental sensing and modelling research unit (ENVISION), Luxembourg Institute of Science and Technology, Belvaux, 4422, Luxembourg
[2] Institute of Geosciences, University of Mainz, 55122, Germany

Correspondence to: Guilhem Türk (guilhem.turk@list.lu)

Abstract. Stable isotopes of oxygen (O) and hydrogen (H) in streams and precipitation are cardinal tools to assess water sources, flow paths, and age. However, their spatial and temporal variability remain largely unknown – essentially due to the limited availability of long-term records of O and H isotope signatures in precipitation. These limitations have stymied their use in studies investigating catchment response to climate change. In this study, O and H isotope signatures are conjectured to be determined by the interplay of physical processes both at synoptic and local scales. Our hypothesis is that large-scale atmospheric circulation patterns (CPs) influence well-known physical effects (e.g., temperature effect) on $\delta^{18}O$ and $\delta^{2}H$ values in precipitation. To test this hypothesis, high-resolution (i.e., sub-daily) $\delta^{18}O$ and $\delta^{2}H$ data were collected in Belvaux (Luxembourg) from 2017 to 2022 to investigate potential relationships with large-scale atmospheric circulation patterns and local-scale meteorological variables.

Our results demonstrate CP controls on precipitation $\delta^{18}O$ and on the relationship between $\delta^{18}O$ and air temperature across Western Europe, with $\delta^{18}O$-temperature ($\delta^{18}O$-T) correlation slopes being larger (0.24 to 0.69) than previously reported (below 0.40). We leveraged CP-specific $\delta^{18}O$-T functions to build a multiple linear regression model for long-term $\delta^{18}O$ reconstructions in Europe, based on geospatial attributes. The model was fitted on GNIP $\delta^{18}O$ data, with a performance expressed by a root mean squared error (RMSE) of 2.3 ‰, comparing to other models focused on the regionalisation of seasonal $\delta^{18}O$ variability over Europe. With this novel method, intramonthly $\delta^{18}O$ in precipitation can be reconstructed for ~150 years by solely relying on historical temperature records (e.g., as obtained from WMO's Climate Explorer web interface (https://climexp.knmi.nl)). Our model offers an assumption-lean and thus robust alternative to reconstruct pre-instrumental precipitation $\delta^{18}O$ chronicles.

https://doi.org/10.5194/egusphere-2024-4169
Preprint. Discussion started: 17 February 2025

1 Introduction

Owing to their near-conservative nature, the stable isotopes of oxygen (O) and hydrogen (H) are powerful tools to investigate water sources, flow paths, and age (Klaus and McDonnell, 2013), as well as catchment response to climate change. Over the last two decades, $\delta^{18}O$ and $\delta^{2}H$ values in precipitation and stream water have been used in a variety of studies unveiling complex and sometimes unexpected streamflow contributions. For example, one-third of the global river discharge has been found to consist of so-called young water, i.e., less than 2–3 months old (Jasechko et al., 2016). Such insights help predicting the effects of the intensification of the hydrologic cycle (Allen and Ingram, 2002; Blöschl et al., 2017, Madakumbura et al., 2019) on the "changing pulse of rivers" (Slater and Wilby, 2017). Long-term $\delta^{18}O$ chronologies are particularly valuable in this respect, because they have been used to understand changes in the hydrologic cycle (Reckerth et al., 2017), and global change impacts on large river systems (Rank et al., 2018). Thus, multi-decadal records of $\delta^{18}O$ values in precipitation and stream water bear considerable potential to answer questions on flood and drought resilience under a changing climate.

However, historic $\delta^{18}O$ datasets in precipitation and in stream water are scarce, and their spatial and temporal variability remain uncertain (Stumpp et al., 2014), shifting the focus to new approaches to retrieve long-term $\delta^{18}O$ chronologies. The Global Network of Isotopes in Precipitation (GNIP) was established in 1960 and holds monthly $\delta^{18}O$ and $\delta^{2}H$ data to the present day, but complete records from the start exist only for a few locations. In 2002, a complementary program called the Global Network of Isotopes in Rivers (GNIR) was initiated, dedicated to the collection, compilation, and dissemination of stream water isotope data (Halder et al., 2015). To overcome the limitations inherent to rather short (in terms of climate change) observation intervals, pre-instrumental $\delta^{18}O$ data can be obtained from environmental archives, such as sediments, ice-cores (Konecky et al., 2020), tree-rings (Álvarez et al., 2024; Rodriguez-Caton et al., 2024) or mollusc shells (Pfister et al., 2018; Schöne et al., 2020). For certain proxies, the temporal resolution of such data can be a limiting factor, mismatching the timescales of hydrological processes. Thus, isotope-enabled numerical climate models (Sturm et al., 2010; Werner et al., 2016), or, more recently, AI models (Nelson et al., 2021), are promising alternatives or complementary to proxy-based approaches. Through the application of reanalysis datasets, e.g., ERA5, which typically span back to the mid-20th century and incorporate measurements from multiple sources, including satellite data since the 1980s, these models can help to reconstruct monthly precipitation $\delta^{18}O$ signals with high accuracy over a large geographical extent.

Recent findings on the role of atmospheric circulation (e.g., moisture sources, air mass trajectories) on precipitation $\delta^{18}O$ signals raise the question on how well models will perform for long-term $\delta^{18}O$ reconstructions. The answer is not straightforward due to the rather short span (~20 years) of available $\delta^{18}O$ calibration data. In the Hubbard brook catchment (New Hampshire, USA), a significant decrease in precipitation $\delta^{18}O$ and $\delta^{2}H$ values observed between 1968 and 2010 has been linked to changes in atmospheric circulation (Puntsag et al., 2016). Along similar lines, a process-based connection was established between isotopic signatures in precipitation and the frequency of strong large-scale ocean water evaporation events in the subpolar North Atlantic (Aemisegger, 2018). Modifications in large-scale movements of air masses need to be incorporated in precipitation $\delta^{18}O$ models, especially for intervals under the influence of climate forcing.

https://doi.org/10.5194/egusphere-2024-4169
Preprint. Discussion started: 17 February 2025

However, many of the processes determining the precipitation $\delta^{18}O$ signal, amongst which atmospheric circulation, occur on much shorter timescales (hours to days) than the standard observation interval for $\delta^{18}O$ in precipitation (weeks to months). Examples of processes occurring at short timescales are interactions at the boundary layer and moisture inputs from evapotranspiration (Aemisegger et al., 2014, 2015), with continental landmasses being occasionally large contributors of recycled moisture in Europe (Insua-Costa et al., 2022). Thus, isotope-enabled climate models are difficult to constrain (Nelson et al., 2021; Sturm et al., 2010), and they often fail in capturing long-term trends caused by changes in atmospheric circulation (Putman et al., 2021). It remains unclear whether this issue can be solved with AI-based approaches, at least as long as the problem of limited calibration isotope chronologies persists. Related uncertainties inherent to the physical causalities could eventually be large when attempting reconstructions of pre-instrumental chronologies.

Fundamental physical effects determining O and H isotope signatures in precipitation have been documented since pioneering work by Dansgaard (1964). The temperature effect, i.e., equilibrium fractionation during condensation following a Rayleigh distillation scheme, is arguably the most important one. A consequence of this process is that the further inland air masses travel, the more negative the $\delta^{18}O$ and $d^{2}H$ signals become due to a gradual depletion of the heavy isotopes (i.e., they condensate and precipitate more easily). Also known as the continental effect, this implies higher variability and amplitudes of the $\delta^{18}O$ and $d^{2}H$ signals in precipitation far from the coast. Latitude and altitude effects also exist, reflecting colder condensation temperature and fast uplifting of moist air masses with strong topographic gradients (i.e., orographic rainfalls).

We hypothesise that daily atmospheric circulation patterns (CPs) influence temporal and spatial features of the well-known physical effects (e.g., temperature effect) on $\delta^{18}O$ and $\delta^{2}H$ values in precipitation. We account for this CP-specific influence in a simplistic modelling approach based on pre-established physical effects. To test our hypothesis and model, we rely on six years of high-resolution (i.e., sub-daily) precipitation $\delta^{18}O$ and $\delta^{2}H$ data, as well as high-resolution meteorological data (hourly temperature and precipitation). Daily synoptic CPs are also considered, derived from a subjective classification scheme. First, we built a model for the relationship between $\delta^{18}O$ and temperature (hereafter referred to as $\delta^{18}O$-T relationship), considering specific CPs based on high-resolution data. Using reanalysis data and geographical attributes, we built a second geospatial model that accounts for the latitude, altitude and continental effects on the seasonal $\delta^{18}O$ (as obtained from the GNIP network in Europe). The combination of the two models is geared towards the reconstruction of up to ~150 years of isotope data in precipitation, based solely on the temperature and variations in CPs.

2 Data and methods

2.1 Sub-daily isotope measurements in precipitation

Sub-daily precipitation data was obtained from a meteorological station located on the rooftop of LIST's (Luxembourg Institute of Science and Technology) premises in Belvaux (49.506630° N, 5.943910° E; WGS84; 305 m asl.). For the sample collection, a modified ISCO automatic liquid sampler with small inserts at the opening of the bottles was used to limit the effects of in-bottle evaporation (Von Freyberg et al., 2020). The inserts, consisting of the outer shell of water syringes, were filled first to

https://doi.org/10.5194/egusphere-2024-4169
Preprint. Discussion started: 17 February 2025

reduce the evaporation through their smaller diameter for small rain amounts. For larger rain amounts, the inserts can spill into the larger bottle, which will also undergo less evaporation because the opening is clogged by the syringe. From December 2016 to March 2020, sampling time intervals varied between 4 and 12 hours. Rain events could thus be split or aggregated during that time.

From April 2020 to the end of the sampling campaign in January 2023, a new sampling protocol was applied where event-based precipitation samples were collected twice per day with a pluviometer installed approx. 200 m away from the original sampling site in Belvaux (49.508270° N, 5.940040° E). When the new (manual) sampling protocol started in April 2020, the type of precipitation (e.g., rain, snow, hail) was also recorded. All water samples were analysed for $\delta^{18}O$ and $\delta^{2}H$ values using a Los Gatos TIWA-45-EP off-axis integrated cavity output spectroscopy laser spectrometer (OA-ICOS). Values are reported in per mil relative to the Vienna Standard Mean Ocean Water 2 standard (VSMOW2) (IAEA, 2017) with an accuracy of 0.2‰ for $\delta^{18}O$ and 0.5‰ for $\delta^{2}H$.

Amplitudes of the monthly, precipitation amount-weighted $\delta^{18}O$ and d-excess signal were calculated using sine wave curve fittings using the non-linear least square *nls()* function in *R*, following the equation provided by Kirchner (2016):

$$c_p(t) = A_p \sin(2\pi t - \varphi f t) + k_p\,, \quad (1)$$

Where $c_p(t)$ is the precipitation $\delta^{18}O$ (or d-excess) timeseries, $A_p$is the amplitude, φ is the phase, and f is the frequency (i.e., the inverse of the phase T) of the signal; k_p is a constant.

2.2 Synoptic atmospheric circulation catalogue

To relate synoptic atmospheric circulation data to the precipitation isotopic signal, the "Katalog der Grosswetterlagen Europas" (GWL) catalogue from Hess and Brezowsky (1952) was used – a daily resolved classification scheme of circulation patterns (CPs) over Germany, starting in 1881. This catalogue is based on expert knowledge and a subjective evaluation of the centres of atmospheric activity, i.e., large high and low-pressure areas located in the Northern Hemisphere around Europe. The three major CPs are: zonal, meridional and mixed circulation (Gerstengarbe and Werner, 2005). Zonal circulation relates to a large-scale high-pressure area located in the subtropical part of the North Atlantic Ocean, leading to a rather smooth West to East atmospheric circulation. Meridional circulation prevails during stationary, blocking high-pressure areas in the latitudes spanning from 50° to 65° N. The axis of the atmospheric circulation is then oriented either from the North, East, or South (three sub-types) towards Central Europe (CE). Mixed CPs are a hybrid circulation type, between zonal and meridional CPs with high-pressure centres deviated northwards towards 50° N. Amongst them are either Southwest or Northwest CPs, or when the activity centres are over CE, high or low over CE CPs are distinguished. This classification scheme captures pathways of the air masses and offers detailed descriptions of the observed systems, as opposed to objective classification systems that are mostly based on statistical approaches (Huth et al., 2016).

https://doi.org/10.5194/egusphere-2024-4169
Preprint. Discussion started: 17 February 2025

2.3 Meteorological observations and reanalysis data

Hourly air temperature [°C] 2 m above ground level was obtained from a nearby meteorological station located in Schifflange (49.513710° N, 6.028375° E) and managed by LIST. To match the resolution of our sub-daily isotopic measurements, median temperatures for the duration of the precipitation event were taken (i.e., the observation interval when the automatic sampler was still in use), hereafter referred to as event temperature. Precipitation [mm] was recorded at hourly intervals in Belvaux with a tipping-bucket rain gauge. To compensate for a time interval of inconsistent rain measurements (September to October 2022), data from another nearby rain gauge were used instead (station Oberkorn, 49.512354° N, 5.900925° E).

2.4 Modelling approach

To put atmospheric circulation at the core of the modelling approach, we extracted $\delta^{18}O$-T functions for each specific CP, based on weighted monthly $\delta^{18}O$ averages regrouping samples from specific CPs. Eight linear regression equations were obtained this way and combined into a model using air temperature as a sole input variable:

$$dO_{rec,i} = a_{CP,i} + b_{CP,i} * temp_i, \quad (2)$$

with $dO_{rec,i}$ being the reconstructed $\delta^{18}O$, $temp_i$ the temperature [°C], and $a_{CP,i}$ and $b_{CP,i}$ CP-dependant coefficients at event-scale for an observation *i*. The model was calibrated on the four years of $\delta^{18}O$ observations before 2021, yielding linear regression estimates for each CP. The model was then validated using the $\delta^{18}O$ data of the years 2021–2022.

To transpose the results from the first model across continental Europe, we built a second geospatial model based on multiple linear regression model fitted on monthly GNIP $\delta^{18}O$. The latitude and longitude were taken as station attributes, while the elevation and air temperature were extracted from the monthly resolved ERA5-Land dataset (0.5° × 0.5° grid). GNIP $\delta^{18}O$ data is unevenly distributed in time and space. To avoid underrepresenting locations with short records, the geospatial model was fitted to the mean seasonal amplitude of the $\delta^{18}O$ signal for stations with at least one full year of observation (N = 233). Considering station latitude, longitude and elevation as geospatial attributes the following equation was obtained:

$$dO_{GNIP,x,j} = c + c_1 * lat_x + c_2 * long_x + c_3 * alt_x + c_4 * dO_{rec,x,j}, \quad (3)$$

With $dO_{GNIP,x,i}$ being the interannual weighted GNIP $\delta^{18}O$ for a station *x* and month *j*, lat_x the latitude [°N], $long_x$ the longitude [°E], alt_x the altitude [masl], and $dO_{rec,x,j}$ the average of reconstructed $\delta^{18}O$ readapting equation 2:

$$dO_{rec,x,j} = \sum_{i=1}^{N_{x,j}} \frac{a_{CP,i}}{N_{x,j}} + \sum_{i=1}^{N_j} \frac{b_{CP,i}}{N_{x,j}} temp_{x,j}, \quad (4)$$

With $temp_j$ being the interannual average monthly temperatures and $N_{x,j}$ the number of days in a month *j*. Two thirds of the stations (N = 156) went into training the geospatial model, yielding values for the constant *c* and coefficients $c_{1,2,3,4}$, while the remaining third of the stations was taken for the validation (N = 77).

Gridded temperature timeseries can then be fed to the model to produce $\delta^{18}O$ maps for continental Europe for any time *j* after 1881, i.e., the starting year of the Hess-Brezowsky catalogue. The extent and the temporal resolution of the modelled $\delta^{18}O$ solely depend on the input temperature data and the spatial resolution of the DEM grid. We used ERA5 reanalysis temperature

https://doi.org/10.5194/egusphere-2024-4169
Preprint. Discussion started: 17 February 2025

data and a 0.5° × 0.5° DEM grid to produce monthly $\delta^{18}O$ isoscapes for Europe starting in 1950. Model performance was assessed by the root mean square error (RMSE) normalized to the standard deviation (SD) of the observed $\delta^{18}O$.

3 Results

3.1 Isotopic variability and $\delta^{18}O$-T relations according to synoptic atmospheric activity

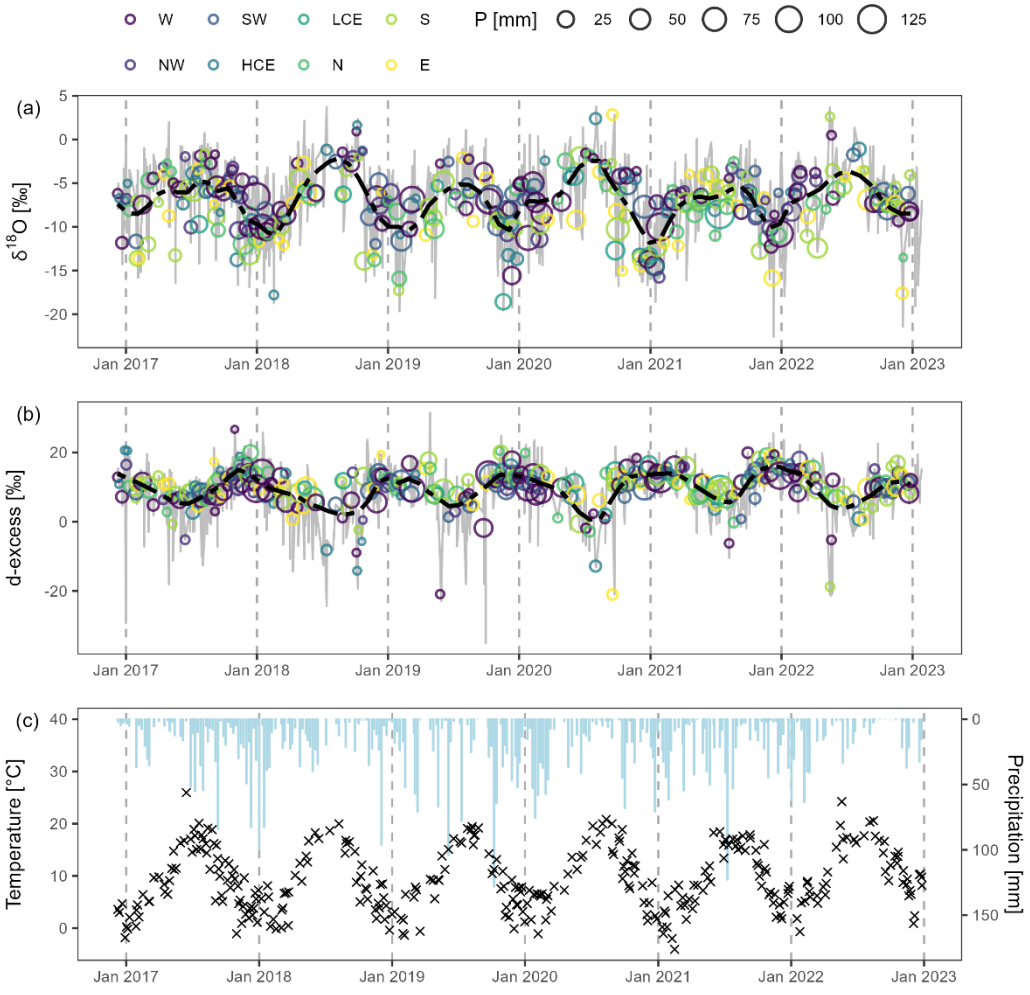

Figure 1: Timeseries of (a) precipitation $\delta^{18}O$, (b) d-excess, and (c) event temperature and precipitation in Belvaux (L) between 2017 and 2022. The grey curves in (a) and (b) represent the sub-daily samples (N = 1630) that were taken, while the coloured circles are weighted means of subsequent samples where the CPs (atmospheric circulation patterns) remained the same. The size of the circles is related to the total precipitation amount of these subsequent samples. The light blue bars in (c) represent the precipitation amount, and the crosses the event temperature for these same subsequent samples. Acronyms used for the CPs are W = West, NW = Northwest, SW = Southwest, HCE = High over Central Europe, LCE = Low over Central Europe, N = North, S = South, E = East, and indicate the direction of the incoming air masses in Germany (as per the Hess-Brezowsky catalogue, 1952).

https://doi.org/10.5194/egusphere-2024-4169
Preprint. Discussion started: 17 February 2025

Taken over the entire sampling interval from December 2016 to December 2022 (1630 samples), the weighted average precipitation $\delta^{18}O$ was -8.1 ‰ with a range of 26.3 ‰, for the d-excess it was 10.7 ‰ with a range of 66.5 ‰. The isotopic signal of precipitation exhibits a distinct seasonality, with inverse patterns for the $\delta^{18}O$ and the d-excess (Figs. 1a and 1b). Average summer high and winter low values were -5.9 ‰ and -9.5 ‰ for $\delta^{18}O$, and 7.6 ‰ and 12.1 ‰ for d-excess values respectively. The intramonthly variability was high, with an average standard deviation of 3.0 ‰ for $\delta^{18}O$ and 5.6 ‰ for d-excess values, close to the seasonal amplitude of the isotope signals. The local meteorological water line (LMWL) was flatter than the global meteorological water line (GMWL) with a slope of 7.54 (versus 8.00, GMWL) and an intercept of 7.0 ‰ (versus 10.0 ‰, GMWL).

The mean annual air temperature during the sampling interval was 10.4 °C – slightly higher than the climatic normal (1991-2020) of 9.9°C in Luxembourg (MeteoLux (https://www.meteolux.lu/fr/climat/normales-et-extremes/), accessed on 14/10/2024). Note that the year 2021 was colder, with a mean annual air temperature of 9.5 °C. Compared to the 2017–2022 mean annual precipitation of 876 mm, rainfall totals were rather high in 2021 (1026 mm) – mostly due to a very wet summer (JJA, 324mm) that led to disastrous flood events in Germany, Belgium and Luxembourg (Fig. 1c). Winter and spring of 2017 were rather dry, with seasonal totals of 72 mm and 78 mm, respectively. The winter of 2019/2020 was rather wet with 420 mm of precipitation.

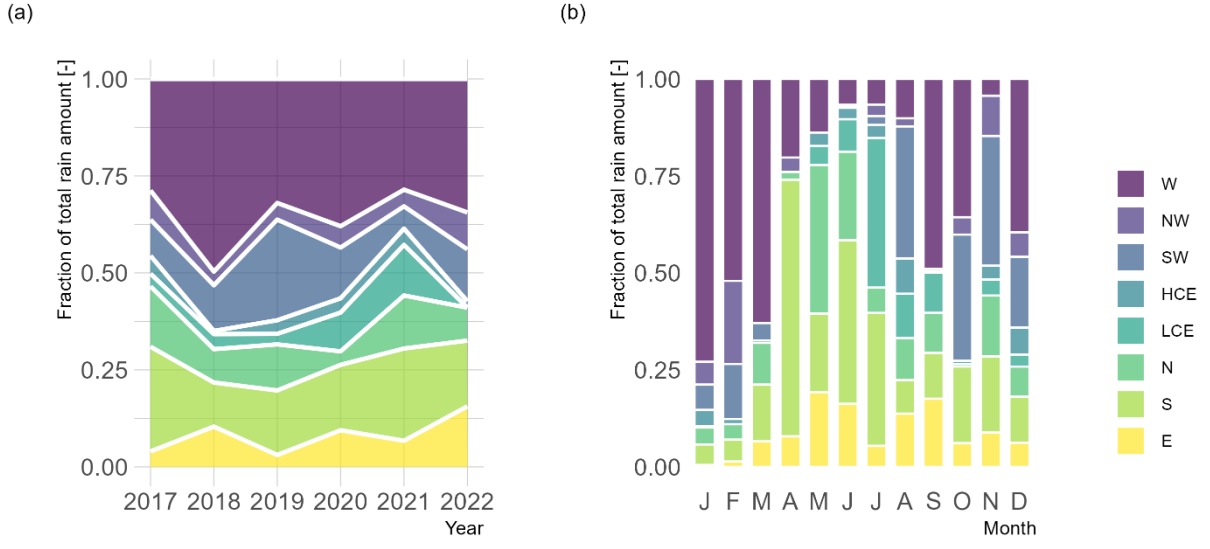

Figure 2: CP distribution over the sampling years from 2017 to 2022. Relative fraction of the CP contribution to (a) the interannual precipitation amount, and (b) the monthly precipitation. For the acronyms used for the CPs, refer to the caption in Fig. 1.

Throughout the sampling interval, approximately half of the annual precipitation originated from western CPs (*W*) – with a notable peak between 2018 and 2020 (Fig. 2a). The origin of precipitation varied seasonally (Fig. 2b), with *W* delivering most precipitation during winter, while contributions from meridional CPs, i.e., North (*N*), South (*S*) and East (*E*), prevailed during

https://doi.org/10.5194/egusphere-2024-4169
Preprint. Discussion started: 17 February 2025

spring and early summer. In summer, CPs were quite variable, and Highs (*HCE*) and Lows over central Europe (*LCE*) delivered considerable amounts of precipitation. Precipitation originating from *W*, common in winter, was almost absent between May and August and in November, while southwestern CPs (*SW*) generated large contributions in precipitation in August and between October and December. Precipitation contributions from *S* were largest from April to June, and from May to July for *N*. In 2017 and in 2021, *S* contributions were quite important – probably due to the large rain amounts in summer, opposed to the dry winter/spring period observed in 2017. *N* and *LCE* contributions were well represented in 2021, while *W* contributions were particularly large during the wet winter of 2018. *SW* circulation contributions were highest in 2019.

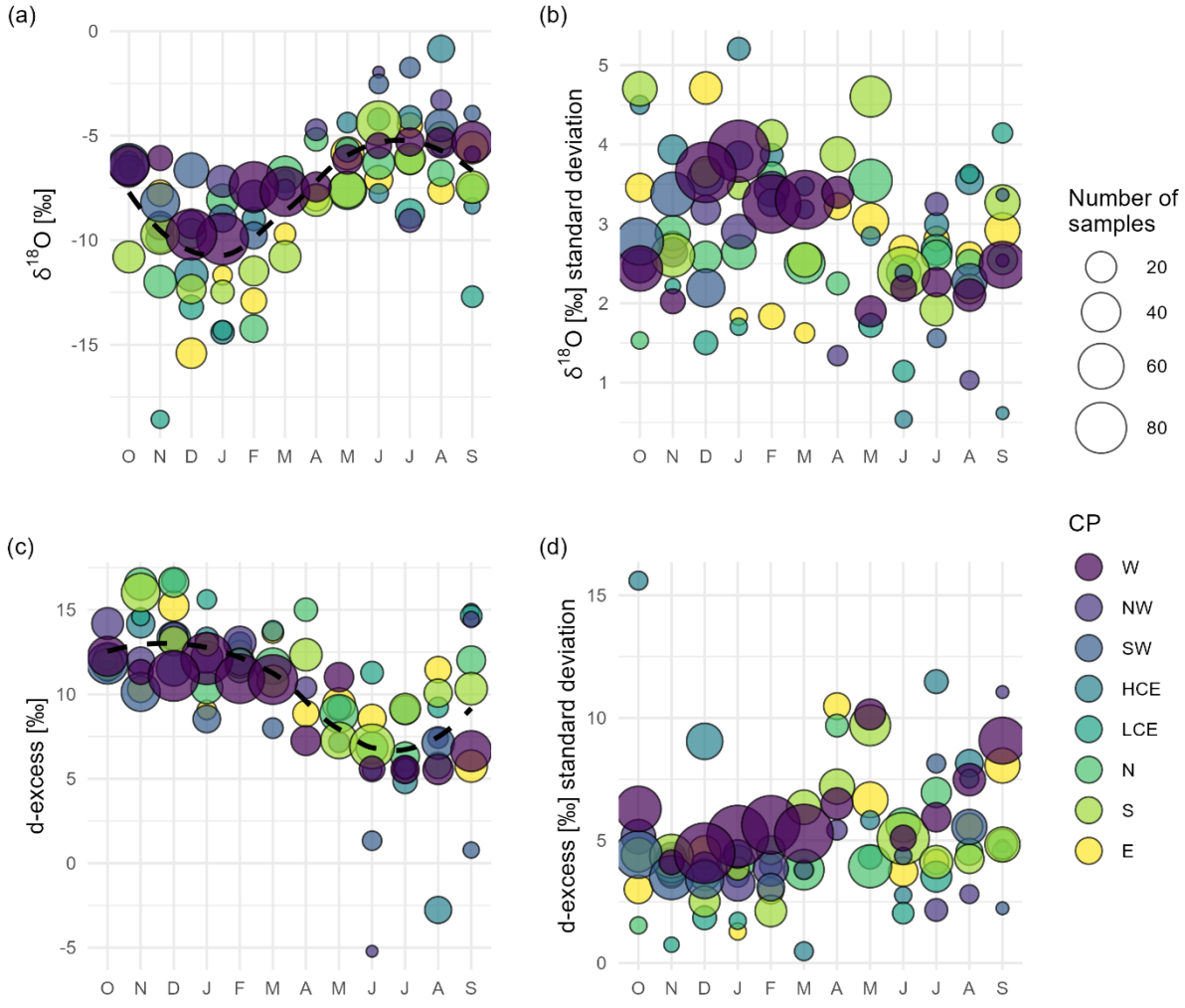

Figure 3: Influence of the CPs on the amplitudes of the seasonal precipitation isotope signal. Monthly amount-averaged (a) precipitation $\delta^{18}O$ and (c) d-excess for samples characterised by specific CPs, and respective standard deviations (b) and (d). The

https://doi.org/10.5194/egusphere-2024-4169
Preprint. Discussion started: 17 February 2025

dot size is proportional to the number of samples; the black dotted line was fitted using a loess-algorithm to emphasise the seasonal trend of the data. For the acronyms used for the CPs, refer to the caption in Fig. 1.

Monthly CP-specific contributions to precipitation show contrasting isotope signals (Fig. 3), which are expressed by phase and amplitude shifts of the sine wave-fitted curves (Tables 1 and 2). The sine wave fitted curve of the $\delta^{18}O$ (without considering CPs) had an intercept of -7.7 ‰ and an amplitude of 2.0 ‰. Likewise, the d-excess curve had an intercept of 10.2 ‰ and an amplitude of 2.5 ‰. For individual CP groups, the $\delta^{18}O$ amplitudes range from 1.4 ‰ to 5.3‰, while values for the d-excess had similar ranges between 2.6 ‰ and 6.6 ‰. Standard deviations of sub-daily $\delta^{18}O$ and d-excess were high for individual months, in some cases exceeding the amplitude of the seasonal isotope signals expressed by the sine wave fits. On average, the intramonthly standard deviation of sub-daily $\delta^{18}O$ was 3.6 ‰ and highest in winter, and 6.0 ‰ for the d-excess and highest in late summer/ beginning of autumn. The LMWL for individual CPs deviated, with slopes comprised between and 7.19 (*HCE*, *E*) to 8.03 (*NW*) and intercepts between 2.5 ‰ (*HCE*) and 12.6 ‰ (*NW*).

Table 1: Amplitude *(A)*, phase *(phi)*, intercept *(k)*, goodness of fit *(R^2)* of the sine wave curves fitted to the weighted monthly $\delta^{18}O$ for each individual CP. For the acronyms used for the CPs, refer to the caption in Fig. 1.

	A [‰]	*phi [months]*	*k [‰]*	*R^2 [-]*
W	2.6	3	-6.7	0.43
NW	1.4	1	-7.2	0.10
SW	2.2	2	-6.6	0.38
HCE	5.3	-98	-7.8	0.69
LCE	5.0	1	-10.5	0.71
N	2.1	2	-8.6	0.33
S	3.6	2	-8.9	0.57
E	3.8	2	-8.6	0.45

When considering individual CP isotope signatures, the zonal CP *W* featured higher $\delta^{18}O$ values, translating into sine wave fits with less negative intercepts (k = -6.7 ‰) and with a moderate amplitude (A = 2.6 ‰) (Table 1). Meridional CPs (*N*, *S* and *E*) had sine wave fits with similar intercepts (k = -8.7 ± 0.2 ‰) and high amplitudes (A = 3.7 ± 0.1 ‰), except for *N* (A = 2.1 ‰). Larger amplitudes of S and E $\delta^{18}O$ resulted from a steep drop of values in winter. $\delta^{18}O$ from *SW* showed more similarities with *W* than with contributions from *S*, while the *NW* $\delta^{18}O$ appeared to be a mixture of *N* and *W* inputs. High amplitudes (A = 5.1 ± 0.1 ‰) were obtained when the centres of atmospheric activity were over Central Europe (*HCE* and *LCE*), with particularly negative $\delta^{18}O$ for *LCE* (k = -10.5 ‰). The phase *phi* always laid in the same range of values between 1 and 3 months for all the CPs, except for *HCE*, where the occurrence of rainless months around the winter period led to the high negative value. Goodness-of-fit values ranged from moderate to high for most of the CPs (R^2 = 0.33 – 0.71), except for the

https://doi.org/10.5194/egusphere-2024-4169
Preprint. Discussion started: 17 February 2025

northwestern CP (*NW*) which had a weak fit (R^2 = 0.10). Still, the intramonthly standard deviation of sub-daily $\delta^{18}O$ within the CPs was high with average values between 1.8 ‰ and 2.7 ‰.

Table 2: Amplitude *(A)*, phase *(phi)*, intercept *(k)* and goodness of fit *(R^2)* of the sine wave curves fitted to the weighted monthly d-excess for each individual CP. Negative correlations of the sub-daily d-excess with $\delta^{18}O$ and their significance were given by the Pearson's rho coefficient (ρ) and corresponding p-values (*p*). For the acronyms used for the CPs, refer to the caption in Fig. 1.

	A [‰]	*phi [months]*	*k [‰]*	*R^2 [-]*	*ρ [-]*	*p [-]*
W	2.6	-1	9.4	0.21	-0.60	< 0.001
NW	-3.2	2	10.4	0.25	-0.12	0.624
SW	-2.6	1	8.9	0.27	-0.34	0.085
HCE	-6.6	3	8.3	0.64	-0.56	0.003
LCE	3.7	11	12.9	0.65	-0.76	0.007
N	-4.2	2	11.5	0.62	-0.36	0.047
S	-3.2	2	11.3	0.40	-0.53	< 0.001
E	3.5	-1	10.7	0.33	-0.54	0.002

The d-excess patterns observed among the different CPs resembled those for the $\delta^{18}O$, with d-excess being negatively correlated to the $\delta^{18}O$ (Pearson's ρ = -0.49, $p < 0.001$). The range of the seasonal d-excess amplitudes (4.0 ‰) grossly matched the range of $\delta^{18}O$ amplitudes (3.9 ‰), with lesser differences between the CPs. High $\delta^{18}O$ value CPs plotted lower with the d-excess because of this anti-correlation, e.g., *W* (k = 9.4 ‰). Note that this negative correlation varies amongst the CP groups, being non-significant for *NW* and *SW*, and weak for *N* (ρ = -0.36, p = 0.047). In the remaining groups, this correlation was stronger, with ρ ranging from -0.53 to -0.76 (Table 2). Goodness of fit ranged from moderate to high (R^2 = 0.21 – 0.65). Again, the intramonthly variation was high, with standard deviations of sub-daily d-excess within the CPs between 3.1 ‰ and 5.0 ‰.

https://doi.org/10.5194/egusphere-2024-4169
Preprint. Discussion started: 17 February 2025

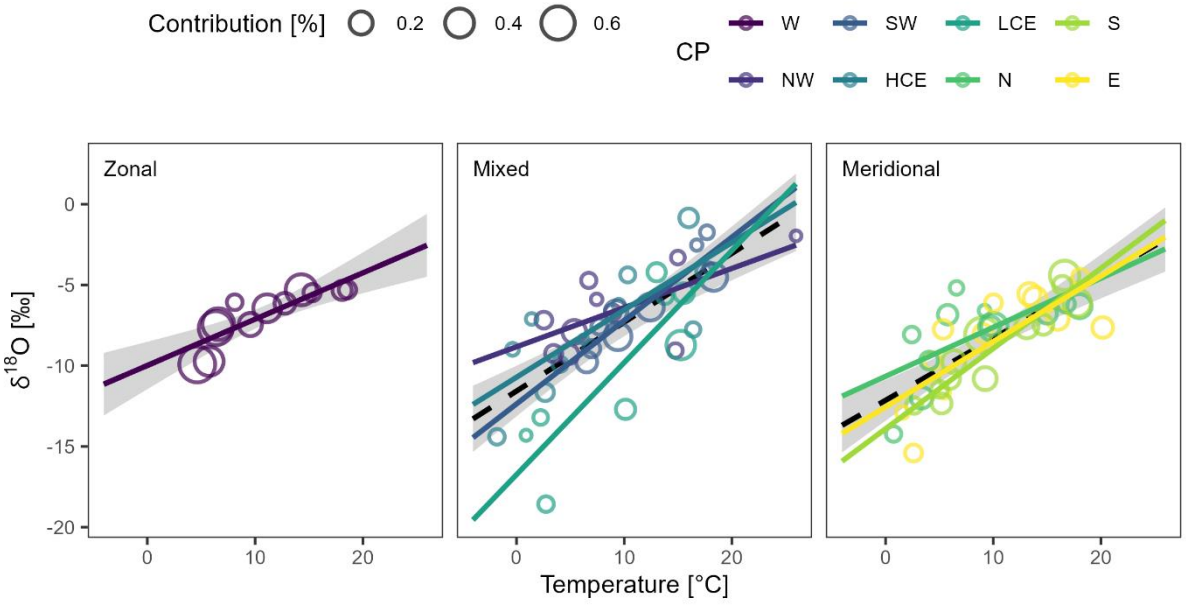

Figure 4: δ^{18}O-T relation according to synoptic atmospheric activity. CP-specific interannual monthly δ^{18}O are plotted against average event temperature, both weighted. The size and the colour of the circles indicates the contribution of the specific CP to the total precipitation amount of each month. Linear regression lines were also fitted to the data – the dotted line, with the grey shading indicating the uncertainty, is the mean line across all the CPs to better visualise the differences. For the acronyms used for the CPs, refer to the caption in Fig. 1.

Next, we investigated the δ^{18}O-T relation under different CPs (Fig. 4). For this, we computed CP-specific interannual means of monthly weighted δ^{18}O and event temperature. Plotting these against each other, we obtained CP-specific δ^{18}O-T linear relationships with slopes ranging from 0.24 ‰/°C (*NW*, *a* = -8.8 ‰) to 0.69 ‰/°C (*LCE*, *a* = -16.8 ‰). The highest and lowest intercepts were also obtained for those same CPs. The average intercept between the CPs was -12.0 ‰ with a slope of 0.42 ‰/°C, which correspond to values obtained for *E*. Higher intercepts and shallower slopes were obtained when the origins of the airmasses were located in the North or West (*W*, *N*, and *NW*). On the contrary, lower intercepts and steeper slopes were obtained when meridional CPs originating from the South dominated (*S* and *SW*). The RMSE ranged from 1.0 ‰ (*S*) to 2.9 ‰ (*LCE*), being 1.50 to 3.60 times lower than the δ^{18}O amplitude (except for *N* and *NW*), and the statistical significance of the δ^{18}O-T linear relations went from moderate (R^2 = 0.47, *NW*) to high (R^2 = 0.88, *S*).

Table 3: Intercept *a*, coefficient *b*, root mean squared error (*RMSE*), goodness of fit (R^2), and signal amplitude to uncertainty ratio (*A/RMSE*) of the CP-specific δ^{18}O-T relations obtained for interannual monthly weighted δ^{18}O. For the acronyms used for the CPs, refer to the caption in Fig. 1.

	a [‰]	*b [‰/°C]*	*RMSE [‰]*	*R^2 [-]*	*A/RMSE [-]*
W	-10.0	0.29	0.9	0.73	2.89
NW	-8.8	0.24	2.0	0.47	0.70

https://doi.org/10.5194/egusphere-2024-4169
Preprint. Discussion started: 17 February 2025

SW	-12.4	0.52	1.1	0.86	2.00
HCE	-10.7	0.42	2.5	0.60	2.12
LCE	-16.8	0.69	2.9	0.72	1.72
N	-10.7	0.30	2.1	0.43	1.00
S	-13.9	0.50	1.0	0.88	3.60
E	-12.6	0.41	2.2	0.59	1.73

3.2 Event-based model to predict precipitation $\delta^{18}O$ in Luxembourg based on CPs

From the model results based on Equation 2 and the linear regression estimates from Table 3, a good reproduction of the seasonal $\delta^{18}O$ (Fig. 5a) and a moderate correlation with observed $\delta^{18}O$ at weekly scale (R^2 = 0.44) can be deduced. The root mean square error (RMSE) of 2.6 ‰ lied well below the standard deviation of weekly $\delta^{18}O$ (3.5‰), indicating a fair performance of the model. For comparison, the same model using only one equation disregarding the CPs, yielded a RMSE of 2.8 ‰ for a R^2 of 0.37. Systematic overestimations towards the lower end of values occurred, which typically correspond to the winter season, and underestimations in summer towards the higher end of the $\delta^{18}O$ spectrum (Fig. 5b). This led the linear regression line of modelled versus observed values to deviate from the 1:1 line.

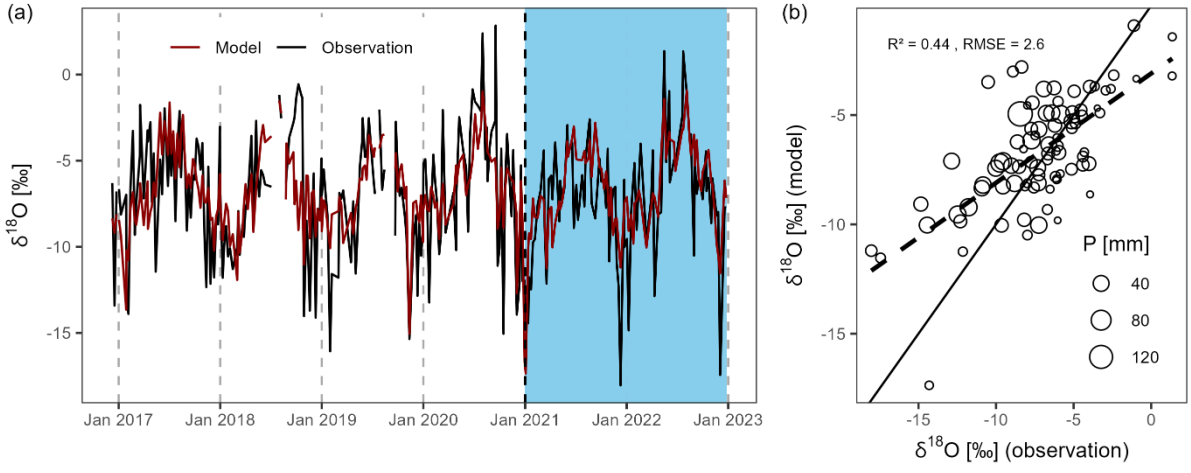

Figure 5: Performance of the event-based model. (a) Timeseries of weekly-resolved modelled $\delta^{18}O$ versus observed $\delta^{18}O$ (N = 275), with the validation period marked by the blue shaded area (N = 89). (b) Scatter plot modelled $\delta^{18}O$ versus the observed $\delta^{18}O$ for the validation period only. The 1:1 line (solid) and a linear regression line (dashed), as well as the goodness of fit (R^2) and the root mean squared error (RMSE) are also shown. The dot size is proportional to the precipitation amount.

https://doi.org/10.5194/egusphere-2024-4169
Preprint. Discussion started: 17 February 2025

3.3 Geospatial model to map the seasonal precipitation $\delta^{18}O$ across GNIP stations in continental Europe

The multiple linear regression model from Equation 3 relying on station latitude, longitude and elevation as geospatial attributes, yielded an average RMSE of 1.4 ‰ for a R^2 of 0.79, when fitted on interannual monthly GNIP $\delta^{18}O$. The normalised RMSE was around 0.50, except for certain coastal areas (Fig. 6).

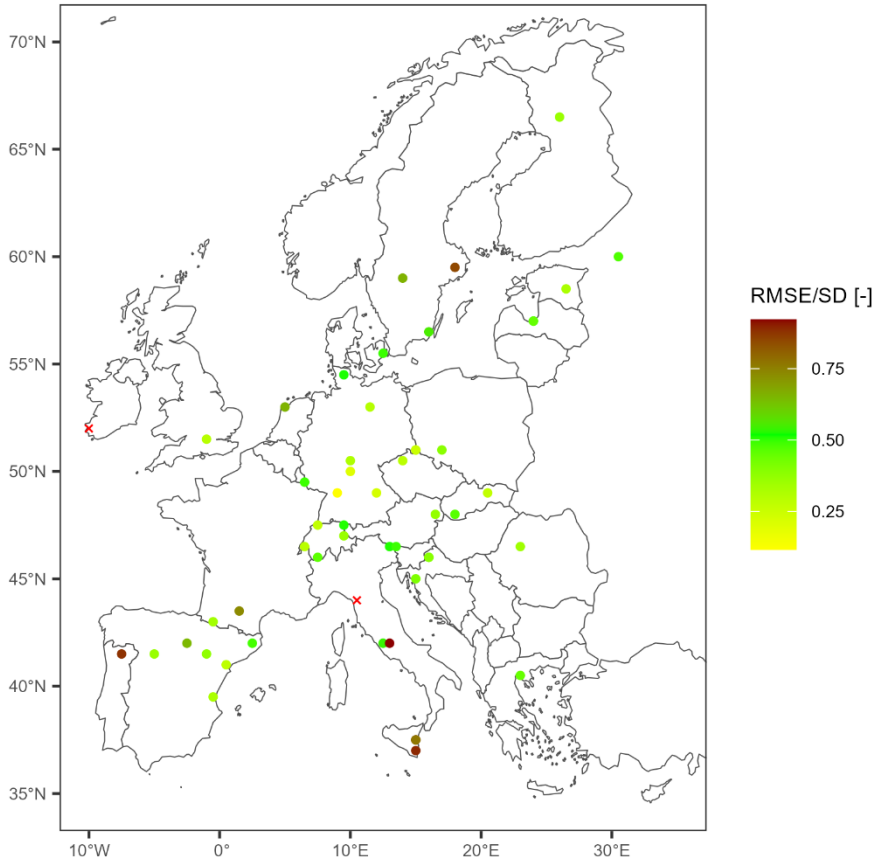

Figure 6: Map of the GNIP stations taken for the validation of the geospatial model (N = 53). The stations were colour-coded according to the root mean squared error normalized to the standard deviation (RMSE/SD). The red crosses indicate locations were the RMSE was greater than the SD.

Table 4: Values of the constant *c* and coefficients of the combined model to produce monthly precipitation $\delta^{18}O$ based on geospatial parameters, synoptic CPs, and local temperature.

	value	*unit*
c	2.8630	‰
c_1	-0.1068	‰/°

https://doi.org/10.5194/egusphere-2024-4169
Preprint. Discussion started: 17 February 2025

c_2	-0.0603	‰/°
c_3	-0.0012	‰/m_{asl}
c_4	0.6149	-

Monthly $\delta^{18}O$ timeseries were modelled introducing monthly ERA5 temperature data in Equation 4, and using the model estimates (Table 4), and yielded an average RMSE of 2.3 ‰ for a R^2 of 0.30 when compared with the GNIP $\delta^{18}O$ in Europe (N = 33,861). The normalised RMSE remained below 1.0 reflecting good performance of the model in Central Europe (Fig. 7). However, towards the coastal areas, values increased (Fig. 7). A slight decrease could also be observed towards higher and lower latitudes of the study area. In a few coastal stations, the RMSE was even larger than the SD. In specific locations, the seasonality of the $\delta^{18}O$ signal was well represented, yet with a systematic underestimation of the amplitude, especially at higher altitude stations in Switzerland, Austria and Germany (Fig. 8). Particularly, the lower end of the $\delta^{18}O$ spectra in winter was poorly represented by the model in these locations, also at the cold climate Rovaniemi station in Finland. Due to the distinct $\delta^{18}O$ seasonality in these colder climates, the R^2 was high (≈0.5). That was not the case at stations with more erratic and less pronounced signals, such as in the Mediterranean (Spain, Portugal and Italy) ($R^2 < 0.28$), and one station in Germany (Trier, $R^2 = 0.14$). The model also performed better for lower altitudes in valleys or plains of Western Europe (Germany and Switzerland) (RMSE < 2.0, $R^2 > 0.52$). The latitude, altitude and continental effects were clearly visible, with lower $\delta^{18}O$ values, e.g., in Northern Europe, the Alps, Pyrenees and the Carpathians, and towards Eastern Europe (Fig. 9). The values were also higher in direct proximity to the Atlantic Ocean and the Mediterranean Sea (Fig. 9).

https://doi.org/10.5194/egusphere-2024-4169
Preprint. Discussion started: 17 February 2025

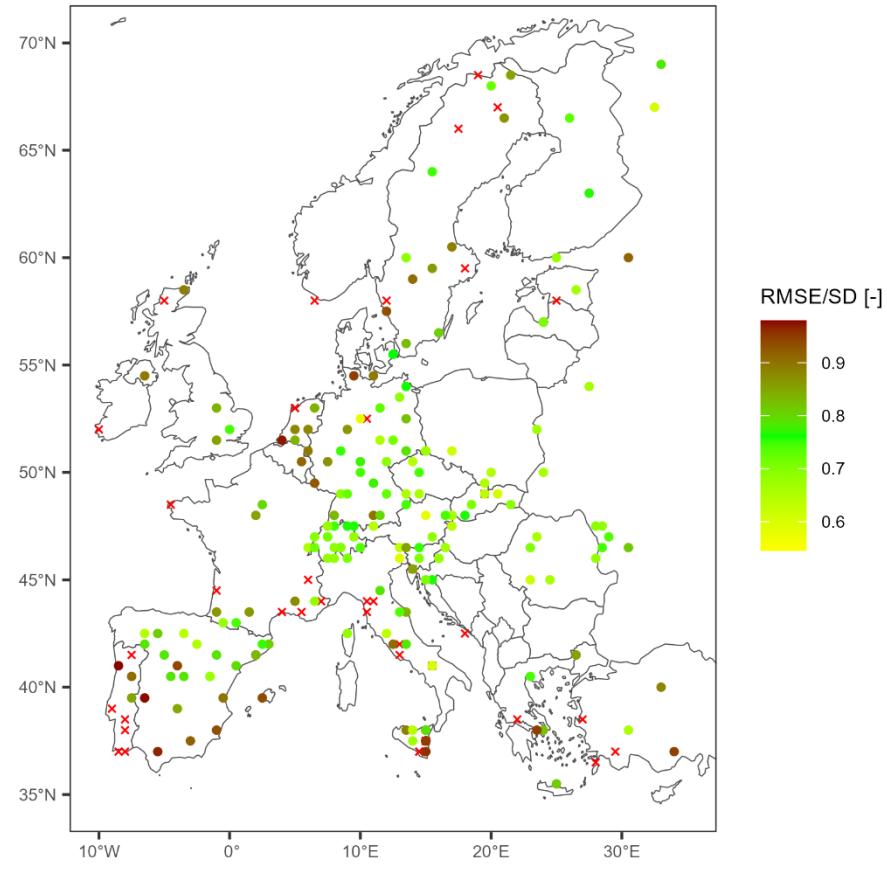

Figure 7: Map of the model performance of the GNIP stations for which monthly $\delta^{18}O$ timeseries were created combining the event-based and the geospatial model. The stations were colour-coded according to the root mean squared error normalised to the standard deviation (RMSE/SD). The red crosses indicate locations were the RMSE was greater than the SD.

https://doi.org/10.5194/egusphere-2024-4169
Preprint. Discussion started: 17 February 2025

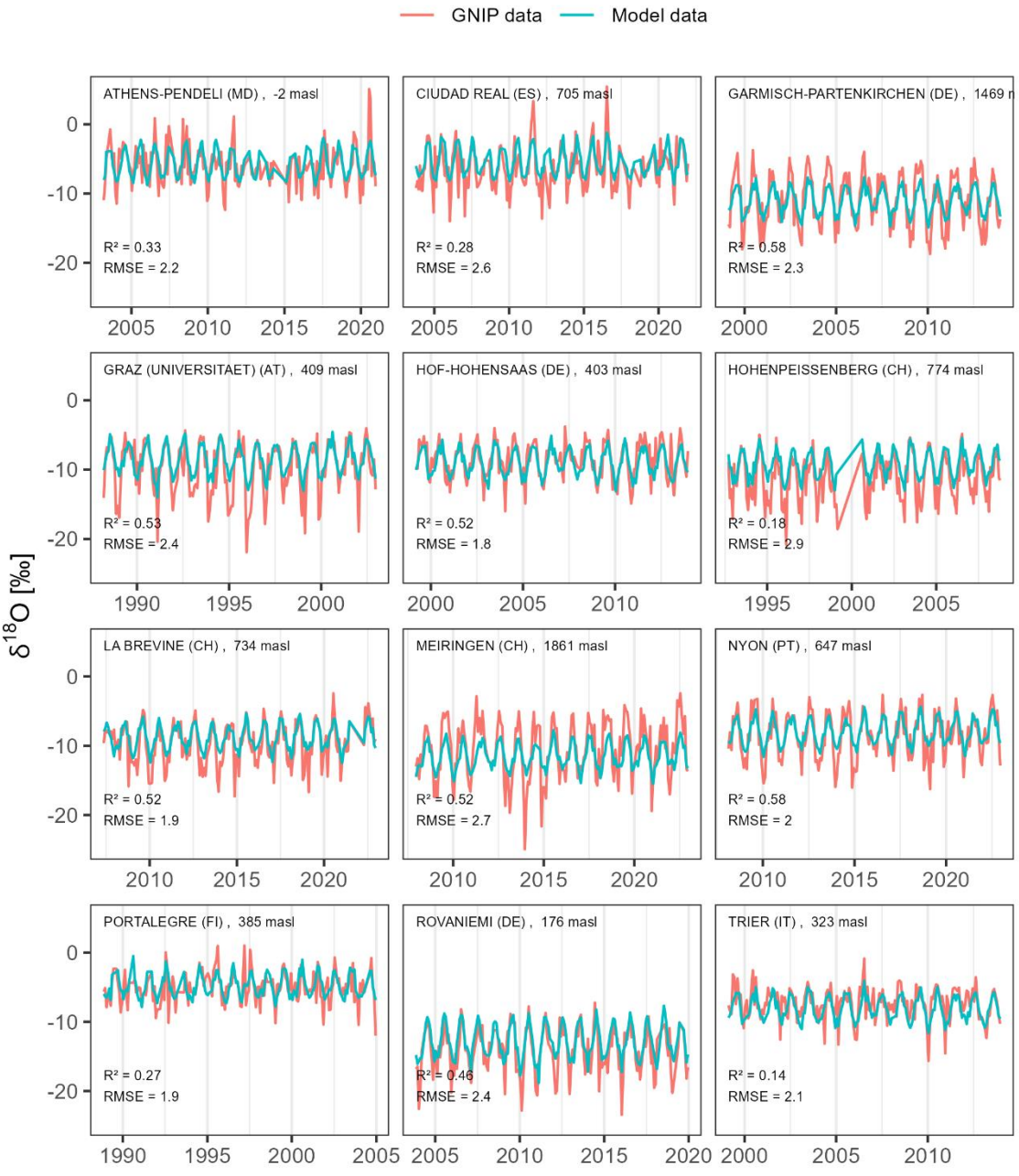

Figure 8: Model performance for 12 locations, selected amongst GNIP stations with over 8 years of observational data (N = 103). The timeseries were truncated for better readability. The performance metrics refer to the entire set of available $\delta^{18}O$ data, not just the data displayed in this figure.

315

https://doi.org/10.5194/egusphere-2024-4169
Preprint. Discussion started: 17 February 2025

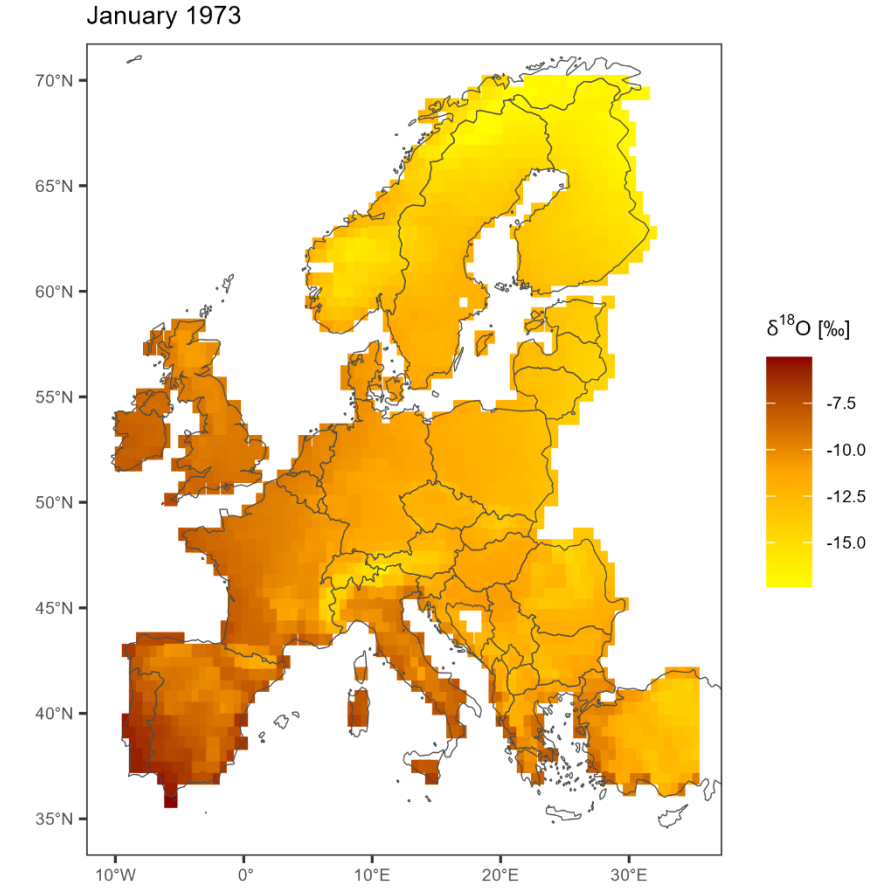

Figure 9: Example of an isoscape generated with the geospatial model in January 1973.

4 Discussion

4.1 Synoptic atmospheric influences on precipitation isotopic signatures and $\delta^{18}O$-T relations

While the mean $\delta^{18}O$ amplitude of 2.0 ‰ for Luxembourg is consistent with seasonal ranges reported in global isoscapes for the same region (Allen et al., 2019), the average weighted $\delta^{18}O$ value (-8.1 ‰) was lower than the long-term mean of 1978 to 2009 at the GNIP station (-7.4 ‰) in Trier, Germany (Stumpp et al., 2014). Judging from the proximity of the stations (~55 km) and small elevation difference (273 m), this is likely not an altitude or latitude effect. However, the Mosel River valley is known for its mild micro-climate, favouring viticulture in the region (Urhausen et al., 2011), which could affect the isotopic signatures in precipitation sampled in Trier.

The isotope signal at both locations showed signs of re-evaporation, i.e., in-cloud evaporation of newly formed raindrops (Moore et al., 2014), with LMWLs less steep than the GMWL (McGuire and McDonnell, 2007). The LMWL slope of 7.54 for

https://doi.org/10.5194/egusphere-2024-4169
Preprint. Discussion started: 17 February 2025

Luxembourg ranks amongst the lowest reported from Germany – solely exceeding stations located in the North (Stumpp et al., 2014). The LMWL was found to vary significantly between dry and wet years, and with changes of the summer temperature (Vodila et al., 2011), which could explain our results, given the unprecedented temperature records during the sampling period. Changes of the convection strength and re-evaporation intensity in the boundary layer, with higher rainfall intensity and frequency in summer, tend to lead to lower $\delta^{18}O$ values (Aemisegger et al., 2015; Moore et al., 2014). Despite the lower LMWL slope, indicating stronger effects of re-evaporation, the weighted d-excess value (10.7 ‰) at the study site was still higher than in Trier (6.3 ‰). This implies that the incoming air moisture in our site had higher d-excess signatures than in Trier before condensation. It is possible that there is a strong recycling of air moisture in the Mosel River valley, causing this difference. Precipitation $\delta^{18}O$ reportedly has a memory effect caused by week-long atmospheric residence times and recycling of water vapour through re-evaporation of raindrops (Moerman et al., 2013).

The d-excess being close to the global mean of 10.0 ‰ following the GMWL, suggests vapour formed over the Atlantic Ocean as a major source of moisture (Celle-Jeanton et al., 2001). This corroborates the fact that $\delta^{2}H$ variations in precipitation in Western Europe are primarily controlled by large-scale rainout processes within landfalling humid air masses deriving from the Atlantic Ocean (Rozanski et al., 1982). The d-excess value is a proxy for evaporation conditions at the moisture source (Merlivat and Jouzel, 1979) and reportedly relates to the remote over-sea relative humidity and the sea surface temperature (Aemisegger et al., 2014; Bonne et al., 2019; Pfahl and Sodemann, 2014). North Atlantic Ocean and land sources over Central Europe have been found to be the main contributors to air moisture in the Northen Alps, with a strong seasonal variability as oceanic sources in winter are tendentially replaced by continental sources in summer (Sodemann and Zubler, 2010). High d-excess values reported here could be caused by continental inputs (Krklec et al., 2018), because continental landmasses can be large contributors of recycled moisture in Europe (Insua-Costa et al., 2022) or air masses from the Mediterranean area (Araguás-Araguás et al., 2000; Celle-Jeanton et al., 2001) that occasionally reach Luxembourg. It should be noted, however, that the isotopic signature of land evapotranspiration significantly varies between seasons, because transpiration from vegetation in summer leads to less negative $\delta^{18}O$ values, closer to or invariant from oceanic input (Krklec et al., 2018).

Accordingly, there is a difference in d-excess (and, to a lesser degree, in $\delta^{18}O$) signatures coming from meridional CPs (*N*, *S*, *E*) with centres of activity on the European continent between 50° and 65°N, and zonal CPs (*W*) influenced by more remote centres of activity over the Atlantic Ocean. These contrasting $\delta^{18}O$ and d-excess contributions depend on the CPs and confirm previous reports on changes of atmospheric circulation influencing precipitation $\delta^{18}O$ (Aemisegger, 2018; Puntsag et al., 2016; Sturm et al., 2010), showcasing their influence in Western Europe. The latter was not evident, considering the dominance of the Atlantic Ocean on precipitation isotope signals (Rozanski et al., 1982; Sodemann and Zubler, 2010). Yet, results suggest that different moisture sources reach Luxembourg, experiencing different levels of complexity during precipitation formation and re-evaporation. Weak or non-significant correlations of $\delta^{18}O$ and d-excess, e.g., for *NW* and *SW*, and *N*, suggest a decoupling of the isotope signal at the moisture origin and the precipitation reaching the study site. High antecedent rainouts as the airmasses travel overland or strong convection could be the cause of this decoupling (Aemisegger et al., 2015; Moore

https://doi.org/10.5194/egusphere-2024-4169
Preprint. Discussion started: 17 February 2025

et al., 2014). *N* and *NW* $\delta^{18}O$ also had a weaker dependency on the temperature, which is interpreted as a lower influence of re-evaporation or contribution of local moisture sources, i.e., continental recycling.

The dependency of $\delta^{18}O$-T functions on CPs validates the hypothesis that CPs affect the physical effects which control precipitation $\delta^{18}O$. The observed temperature effect lied within the range of values reported for Europe, although it is interesting that some CP-specific $\delta^{18}O$-T functions can have slopes usually observed at continental or high-altitude sites. Slopes around or over 0.40 are characteristic for Germany and the Swiss Alps (Rozanski et al., 1992; Stumpp et al., 2014) or Central Europe (Vodila et al., 2011). With slopes over 0.50, *S*, *SW* and *LCE* are the most striking examples. A possible explanation for this similarity lies in the long travel distances of these airmasses over continents and mountain ranges or other sorts of orographic obstacles. This could cause high overland rainouts, combined with large contributions of continental recycling, comparable to landlocked/alpine sites. Broader amplitudes of *S* and *E* $\delta^{18}O$, characteristic of locations far from the coast (McGuire and McDonnell, 2007), also support this explanation. For E, contributions from the Eastern European continent are obvious. The strong $\delta^{18}O$-T relationship for *LCE* is difficult to interpret as the moisture can be associated with multiple high-pressure systems to the West, North or East (Gerstengarbe and Werner, 2005).

Our results confirm the need to review the assumption of a stable $\delta^{18}O$ relation with temperature. This stationarity is now challenged in palaeothermometry suggesting changing $\delta^{18}O$ -T relationships existed in past climates (Jouzel, 1999; Buizert et al., 2014). The temporal $\delta^{18}O$ -T gradient may have been substantially lower for the LGM – Pre-Industrial (LGM-PI) climate changes than the modern one determined for most mid to high-latitude regions (Werner et al., 2016). As shown by many studies, under colder climates (e.g., Last Glacial Maximum, LGM), the $\delta^{18}O$ values in precipitation were lower (Lee et al., 2008; Risi et al., 2010; Werner et al., 2016). Yet , Noone and Simmonds (2002) have shown that only less than 20 percent of the variance in precipitation $\delta^{18}O$ values can be explained by changes in air temperature alone.

4.2 Long-term precipitation $\delta^{18}O$ reconstructions considering atmospheric circulation

The model results with a RMSE of 2.3 ‰ compare well to model performances of published numerical models used for the regionalisation of seasonal $\delta^{18}O$ variability in Europe (Nelson et al., 2021). Very likely this finding can be attributed to the similar structure and the same GNIP dataset used for the calibration. There is some uncertainty in the model, with the $\delta^{18}O$ variability being at least twice as large as the RMSE. Although the model presented here is outperformed by the recent machine learning aided model Piso.AI (RMSE = 1.7 ‰) (Nelson et al., 2021), it has several advantages, namely its simple and flexible structure using only a few variables. Furthermore, the new model relies on established physical effects, assuring continuity in long-term $\delta^{18}O$ reconstructions with limited artifacts. Another strength of the new model is that it can be resolved at multiple temporal scales depending on the resolution of the available variables. Thus, sub-monthly precipitation $\delta^{18}O$ data can be reconstructed starting from 1881, i.e., the starting year of the Hess-Brezowsky catalogue, provided historical temperature records exist at the target location and for the desired temporal resolution. Such data can be accessed, e.g., through the WMO Climate Explorer web interface (https://climexp.knmi.nl) where daily and monthly temperature and precipitation records

https://doi.org/10.5194/egusphere-2024-4169
Preprint. Discussion started: 17 February 2025

starting in the late 19th century can be found. When daily precipitation records are available, the model can be further refined by substituting *N*, i.e., the number of days in a month, in Equation 4 by the precipitation amount. This way, only days with actual precipitation are accounted for and the modelled $\delta^{18}O$ are weighted, further improving the results. When applied to Luxembourg at the weekly scale with higher resolution data, the model performed well with a RMSE of 2.6 ‰, lower than the standard deviation of 3.5 ‰.

By including the atmospheric circulation in the new model, its performance was improved, albeit to a limited extend. When comparing event-based model results at the weekly scale using CP-specific equations and model results and disregarding the CPs, the RMSE was reduced (0.2 ‰) and a higher explained variability was achieved ($R^2 = 0.44$; $\Delta = 0.07$). The moderate improvement by including the CPs into the model could have several reasons, including the rather similar CP distribution throughout the six years of observations (Fig. 2). More variation in the CP behaviour would likely have led to more contrasting results and better performances with the CP-specific model. Another reason for the limited improvement of the model performance by including CPs also lies in the uneven seasonal distribution of the CPs, with an over-representation of certain months and lack of observations in others, e.g., *HCE* and *LCE* were barely captured in the winter. This could also have led to the systematic over- and underestimations towards the lower and higher end of precipitation $\delta^{18}O$ values, especially when considering the complexity of processes during precipitation formation (Aemisegger et al., 2015; Moore et al., 2014). Piso.AI considers convection strength amongst the important predictor variables in the model algorithm (Nelson et al., 2021). This part is missing in the model presented here and certainly explains why the AI model performs better at times. Longer observation intervals covering all CP types at different times of the year and the inclusion of variables accounting for the complex processes during precipitation formation, such as the convection strength, are proposed as direct improvements that could be made to the model.

Despite the overall satisfactory results of the model, it performed in a contrasting way across space, with a high performance in Central Europe, gradually decreasing towards coastal, high altitude or continental areas. Air moisture from the Mediterranean Sea travelling northward to higher latitudes is reportedly intercepted by the Alps acting as an effective barrier (Sodemann and Zubler, 2010), which could explain the poor model performance south of the Alps, e.g., in Italy. Adjusted to inflow of air masses over Luxembourg, the model might not be adapted to parts of Europe where the Mediterranean Sea is a large air moisture contributor, having a significantly different isotopic signature (Celle-Jeanton et al., 2001). In addition to unique isotope signatures in the Mediterranean Basin, the oceanic influence at other coastal locations leads to milder climates that are known to attenuate the $\delta^{18}O$ signal (McGuire and McDonnell, 2007), which the model can barely capture. The opposite can be observed at higher altitudes and in continental sites far inland to the East where a strong $\delta^{18}O$ seasonality prevails. At such sites, the model worked well. Extreme values and high amplitudes are underestimated, leading to low RMSE/SD ratios that indicate a poorer performance. This likely results from conditions that differ significantly from those in Luxembourg, and which have been used to calibrate the model. Having the same CP-specific $\delta^{18}O$-T equations fitted to other coastal, continental and higher altitude sites in Europe, offer new research perspectives to assess how these relationships change over large areas.

https://doi.org/10.5194/egusphere-2024-4169
Preprint. Discussion started: 17 February 2025

5 Conclusions

By using a rare set of sub-daily precipitation $\delta^{18}O$ values covering nearly six years, this study demonstrated that atmospheric circulation patterns (CPs) affect the precipitation isotope signal and $\delta^{18}O$-T functions, i.e., the effect of temperature on $\delta^{18}O$ in precipitation, as measured in Belvaux (Luxembourg). These CP-specific $\delta^{18}O$-T functions were then used to build a multiple linear regression model for long-term $\delta^{18}O$ reconstructions in Europe based on geospatial attributes fitted to GNIP $\delta^{18}O$. More specifically we found:

(i) Signs of in-cloud re-evaporation of newly formed raindrops. This was indicated by the shallow slope (7.54) of the local meteorologic water line (LMWL), which is amongst the lowest in Europe.

(ii) The Atlantic Ocean is a major contributor to precipitation isotope signals in Luxembourg, with an average $\delta^{18}O$ value of -8.1 ‰ and d-excess value of 10.7 ‰.

(iii) A clear difference in $\delta^{18}O$ and d-excess signatures coming from meridional CPs with centres of activity across the European continent between 50° and 65°N, and zonal CPs influenced by more remote centres of activity over the Atlantic Ocean.

(iv) CP-specific $\delta^{18}O$ -T functions with slopes ranging between 0.24 and 0.69. These values are more characteristic of continental or high-altitude sites with typical values of around 0.40. This could result from some CPs having high overland rainouts, together with large contributions of continental recycling, demonstrating the complex contributions to precipitation in Western Europe.

Model performances (RMSE = 2.3 ‰) reported in the present study compared well with other numerical models that focused on the regionalisation of seasonal $\delta^{18}O$ variability in Europe. The new model came with a reasonably low uncertainty with the $\delta^{18}O$ variability at least twice as large as the RMSE. However, the performance of the new model decreased towards coastal, high altitude and continental areas. This was attributed to the fact that the model was calibrated on high-resolution $\delta^{18}O$ from Luxembourg, where meteorological conditions (e.g., temperature variability, precedent rainout effects, air moisture sources) deviate significantly from these locations. The integration of atmospheric circulation in the model resulted in a slight improvement in performance (RMSE reduction of 0.2 ‰) – likely due to similar CP distribution throughout the observation period and uneven seasonal distribution. During our monitoring period, some CPs were overrepresented in certain months, and there was a lack of observations in others, highlighting opportunities for future refinement in addressing these temporal biases. The main advantage of the new model lies in its simple and flexible structure and the low number of required input variables. The model relies on well-known physical effects, ensuring robust long-term $\delta^{18}O$ reconstructions with limited artifacts. Furthermore, it can be applied to multiple temporal scales subject to the resolution of available input data. We propose a novel framework for reconstructing intramonthly $\delta^{18}O$ values in precipitation since 1881, using only historical temperature records at any resolution of interest. Such data can be accessed via the WMO Climate Explorer web interface (https://climexp.knmi.nl). Further improvements of the performance of the new model can be anticipated as more high-resolution observations of $\delta^{18}O$ in precipitation will become available in the coming years. It may also be considered to include variables accounting for the

https://doi.org/10.5194/egusphere-2024-4169
Preprint. Discussion started: 17 February 2025

complex processes during precipitation formation, e.g., the convection strength. Having the same CP-specific $\delta^{18}O$-T equations fitted to other locations in Europe in coastal, continental and higher altitude sites, may also help the model to perform better and offer new perspectives to assess how such relationships change geospatially.

From a user perspective, the new model comes in complement to other available tools to reconstruct pre-instrumental $\delta^{18}O$ signals in precipitation, a recent example being the machine learning Piso.AI model. The strong performance in reproducing precipitation $\delta^{18}O$ by the latter model is traded here for flexibility and reliance on only a few input variables. This is a unique asset when working with less dense environmental records. The new model therefore offers an assumption-lean and robust alternative for reconstructing precipitation $\delta^{18}O$ chronicles into pre-instrumental times.

Author contribution

LP and BRS conceptualized, administrated and supervised the project. They were also responsible for writing the project proposal and acquiring the funding. LP collected and curated the data, which was analysed for the model production by GT, validated by LP. GT wrote the manuscript, which was reviewed and edited by all co-authors.

Competing interests

Some authors are members of the editorial board of journal Hydrology and Earth System Sciences.

References

Aemisegger, F.: On the link between the North Atlantic storm track and precipitation deuterium excess in Reykjavik, Atmos. Sci. Lett., 19, 1–9, https://doi.org/10.1002/asl.865, 2018.

Aemisegger, F., Pfahl, S., Sodemann, H., Lehner, I., Seneviratne, S. I., and Wernli, H.: Deuterium excess as a proxy for continental moisture recycling and plant transpiration, Atmos. Chem. Phys., 14, 4029–4054, https://doi.org/10.5194/acp-14-4029-2014, 2014.

Aemisegger, F., Spiegel, J. K., Pfahl, S., Sodemann, H., Eugster, W., and Wernli, H.: Isotope meteorology of cold front passages: A case study combining observations and modeling, Geophys. Res. Lett., 42, 5652–5660, https://doi.org/10.1002/2015GL063988, 2015.

Allen, M. R. and Ingram, W. J.: Constraints on future changes in climate and the hydrologic cycle, Nature, 419, 224–232, https://doi.org/10.1038/nature01092, 2002.

Allen, S. T., Jasechko, S., Berghuijs, W. R., Welker, J. M., Goldsmith, G. R., and Kirchner, J. W.: Global sinusoidal seasonality in precipitation isotopes, Hydrol. Earth Syst. Sci., 23, 3423–3436, https://doi.org/10.5194/hess-23-3423-2019, 2019.

https://doi.org/10.5194/egusphere-2024-4169
Preprint. Discussion started: 17 February 2025

Álvarez, C., Christie, D. A., González-Reyes, Á., Veblen, T. T., Helle, G., LeQuesne, C., Rodriguez-Caton, M., Szejner, P., Flores-Sáez, F., Gipoulou-Zúñiga, T., Suazo-Álvarez, M., Muñoz-Salazar, T., Aliste, D., Morales, M. S., Muñoz, A., and Villalba, R.: Hydroclimate variability in the Tropical Andes recorded by δ18O isotopes from a new network of Polylepis tarapacana tree-rings, Glob. Planet. Change, 239, https://doi.org/10.1016/j.gloplacha.2024.104503, 2024.

Araguás-Araguás, L., Froehlich, K., and Rozanski, K.: Deuterium and oxygen-18 isotope composition of precipitation and atmospheric moisture, Hydrol. Process., 14, 1341–1355, https://doi.org/10.1002/1099-1085(20000615)14:8<1341::AID-HYP983>3.3.CO;2-Q, 2000.

Blöschl, G., Hall, J., Parajka, J., Perdigão, R. A. P., Merz, B., Arheimer, B., Aronica, G. T., Bilibashi, A., Bonacci, O., Borga, M., Čanjevac, I., Castellarin, A., Chirico, G. B., Claps, P., Fiala, K., Frolova, N., Gorbachova, L., Gül, A., Hannaford, J., Harrigan, S., Kireeva, M., Kiss, A., Kjeldsen, T. R., Kohnová, S., Koskela, J. J., Ledvinka, O., Macdonald, N., Mavrova-Guirguinova, M., Mediero, L., Merz, R., Molnar, P., Montanari, A., Murphy, C., Osuch, M., Ovcharuk, V., Radevski, I., Rogger, M., Salinas, J. L., Sauquet, E., Šraj, M., Szolgay, J., Viglione, A., Volpi, E., Wilson, D., Zaimi, K., and Živković, N.: Changing climate shifts timing of European floods, Science, 357, 588–590, https://doi.org/10.1126/science.aan2506, 2017.

Bonne, J. L., Behrens, M., Meyer, H., Kipfstuhl, S., Rabe, B., Schönicke, L., Steen-Larsen, H. C., and Werner, M.: Resolving the controls of water vapour isotopes in the Atlantic sector, Nat. Commun., 10, 1–10, https://doi.org/10.1038/s41467-019-09242-6, 2019.

Buizert, C., Gkinis, V., Severinghaus, J. P., He, F., Lecavalier, B. S., Kindler, P., Leuenberger, M., Carlson, A. E., Vinther, B., Masson-Delmotte, V., White, J. W. C., Liu, Z., Otto-Bliesner, B., and Brook, E. J.: Greenland temperature response to climate forcing during the last deglaciation, Science, 345, 1177–1180, https://doi.org/10.1126/science.1254961, 2014.

Celle-Jeanton, H., Travi, Y., and Blavoux, B.: Isotopic typology of the precipitation in the Western Mediterranean region at the three different time scales, Geophys. Res. Lett., 28, 1215–1218, https://doi.org/10.1029/2000GL012407, 2001.

Dansgaard, W.: Stable isotopes in precipitation, Tellus, 16, 436–468, https://doi.org/10.3402/tellusa.v16i4.8993, 1964.

Von Freyberg, J., L. A. Knapp, J., Rücker, A., and W. Kirchner, J.: Technical note: Evaluation of a low-cost evaporation protection method for portable water samplers, Hydrol. Earth Syst. Sci., 24, 5821–5834, https://doi.org/10.5194/hess-24-5821-2020, 2020.

Gerstengarbe, F. W. and Werner, P. C.: Katalog der Grosswetterlagen Europas (1881-2004): Nach Paul Hess und Helmut Brezowsky 6., verbesserte und ergänzte Auflage, PIK Rep., 1–148, 2005.

Halder, J., Terzer, S., Wassenaar, L. I., Araguás-Araguás, L. J., and Aggarwal, P. K.: The Global Network of Isotopes in Rivers (GNIR): Integration of water isotopes in watershed observation and riverine research, Hydrol. Earth Syst. Sci., 19, 3419–3431, https://doi.org/10.5194/hess-19-3419-2015, 2015.

Huth, R., Beck, C., and Kučerová, M.: Synoptic-climatological evaluation of the classifications of atmospheric circulation patterns over Europe, Int. J. Climatol., 36, 2710–2726, https://doi.org/10.1002/joc.4546, 2016.

Insua-Costa, D., Senande-Rivera, M., Llasat, M. C., and Miguez-Macho, G.: The central role of forests in the 2021 European floods, Environ. Res. Lett., 17, https://doi.org/10.1088/1748-9326/ac6f6b, 2022.

https://doi.org/10.5194/egusphere-2024-4169
Preprint. Discussion started: 17 February 2025

Jasechko, S., Kirchner, J. W., Welker, J. M., and McDonnell, J. J.: Substantial proportion of global streamflow less than three months old, Nat. Geosci., 9, 126–129, https://doi.org/10.1038/ngeo2636, 2016.

Jouzel, J.: Calibrating the Isotopic Paleothermometer, Science, 286, 910–911, https://doi.org/10.1126/science.286.5441.910, 1999.

Klaus, J. and McDonnell, J. J.: Hydrograph separation using stable isotopes: Review and evaluation, J. Hydrol., 505, 47–64, https://doi.org/10.1016/j.jhydrol.2013.09.006, 2013.

Konecky, B. L., McKay, N. P., Churakova, O. V., Comas-Bru, L., Dassié, E. P., DeLong, K. L., Falster, G. M., Fischer, M. J., Jones, M. D., Jonkers, L., Kaufman, D. S., Leduc, G., Managave, S. R., Martrat, B., Opel, T., Orsi, A. J., Partin, J. W., Sayani, H. R., Thomas, E. K., Thompson, D. M., Tyler, J. J., Abram, N. J., Atwood, A. R., Cartapanis, O., Conroy, J. L., Curran, M. A., Dee, S. G., Deininger, M., Divine, D. V., Kern, Z., Porter, T. J., Stevenson, S. L., von Gunten, L., Braun, K., Carré, M., Incarbona, A., Kaushal, N., Klaebe, R. M., Kolus, H. R., Mortyn, P. G., Moy, A. D., Roop, H. A., Sicre, M. A., and Yoshimura, K.: The Iso2k database: A global compilation of paleo-δ18O and δ2H records to aid understanding of Common Era climate, Earth Syst. Sci. Data, 12, 2261–2288, https://doi.org/10.5194/essd-12-2261-2020, 2020.

Krklec, K., Domínguez-Villar, D., and Lojen, S.: The impact of moisture sources on the oxygen isotope composition of precipitation at a continental site in central Europe, J. Hydrol., 561, 810–821, https://doi.org/10.1016/j.jhydrol.2018.04.045, 2018.

Lee, J.-E., Fung, I., DePaolo, D. J., and Otto-Bliesner, B.: Water isotopes during the Last Glacial Maximum: New general circulation model calculations, J. Geophys. Res., 113, 1–15, https://doi.org/10.1029/2008jd009859, 2008.

Madakumbura, G. D., Kim, H., Utsumi, N., Shiogama, H., Fischer, E. M., Seland, Ø., Scinocca, J. F., Mitchell, D. M., Hirabayashi, Y., and Oki, T.: Event-to-event intensification of the hydrologic cycle from 1.5 °C to a 2 °C warmer world, Sci. Rep., 9, 1–8, https://doi.org/10.1038/s41598-019-39936-2, 2019.

McGuire, K. and McDonnell, J.: Stable Isotope Tracers in Watershed Hydrology, in: Stable Isotopes in Ecology and Environmental Science, Blackwell Publishing Ltd, Oxford, UK, 334–374, https://doi.org/10.1002/9780470691854.ch11, 2007.

Merlivat, L. and Jouzel, J.: Global climatic interpretation of the deuterium-oxygen 16 relationship for precipitation., J. Geophys. Res., 84, 5029–5033, https://doi.org/10.1029/JC084iC08p05029, 1979.

Moerman, J. W., Cobb, K. M., Adkins, J. F., Sodemann, H., Clark, B., and Tuen, A. A.: Diurnal to interannual rainfall δ18O variations in northern Borneo driven by regional hydrology, Earth Planet. Sci. Lett., 369–370, 108–119, https://doi.org/10.1016/j.epsl.2013.03.014, 2013.

Moore, M., Kuang, Z., and Blossey, P. N.: A moisture budget perspective of the amount effect, Geophys. Res. Lett., 41, 1329–1335, https://doi.org/10.1002/2013GL058302, 2014.

Muñoz Sabater, J.: ERA5-Land hourly data from 1950 to present. Copernicus Climate Change Service (C3S) Climate Data Store (CDS). doi: 10.24381/cds.e2161bac (Accessed on 14-10-2024), 2019.

https://doi.org/10.5194/egusphere-2024-4169
Preprint. Discussion started: 17 February 2025

Nelson, D. B., Basler, D., and Kahmen, A.: Precipitation isotope time series predictions from machine learning applied in Europe, Proc. Natl. Acad. Sci. U. S. A., 118, https://doi.org/10.1073/pnas.2024107118, 2021.

Noone, D. and Simmonds, I.: Associations between δ18O of water and climate parameters in a simulation of atmospheric circulation for 1979-95, J. Clim., 15, 3150–3169, https://doi.org/10.1175/1520-0442(2002)015<3150:ABOOWA>2.0.CO;2, 2002.

Pfahl, S. and Sodemann, H.: What controls deuterium excess in global precipitation?, Clim. Past, 10, 771–781, https://doi.org/10.5194/cp-10-771-2014, 2014.

Pfister, L., Thielen, F., Deloule, E., Valle, N., Lentzen, E., Grave, C., Beisel, J. N., and McDonnell, J. J.: Freshwater pearl mussels as a stream water stable isotope recorder, Ecohydrology, 11, 1–10, https://doi.org/10.1002/eco.2007, 2018.

Puntsag, T., Mitchell, M. J., Campbell, J. L., Klein, E. S., Likens, G. E., and Welker, J. M.: Arctic Vortex changes alter the sources and isotopic values of precipitation in northeastern US, Sci. Rep., 6, 1–9, https://doi.org/10.1038/srep22647, 2016.

Putman, A. L., Bowen, G. J., and Strong, C.: Local and Regional Modes of Hydroclimatic Change Expressed in Modern Multidecadal Precipitation Oxygen Isotope Trends, Geophys. Res. Lett., 48, 1–10, https://doi.org/10.1029/2020GL092006, 2021.

Rank, D., Wyhlidal, S., Schott, K., Weigand, S., and Oblin, A.: Temporal and spatial distribution of isotopes in river water in Central Europe: 50 years experience with the Austrian network of isotopes in rivers, Isotopes Environ. Health Stud., 54, 115–136, https://doi.org/10.1080/10256016.2017.1383906, 2018.

Reckerth, A., Stichler, W., Schmidt, A., and Stumpp, C.: Long-term data set analysis of stable isotopic composition in German rivers, J. Hydrol., 552, 718–731, https://doi.org/10.1016/j.jhydrol.2017.07.022, 2017.

Risi, C., Bony, S., Vimeux, F., and Jouzel, J.: Water-stable isotopes in the LMDZ4 general circulation model: Model evaluation for present-day and past climates and applications to climatic interpretations of tropical isotopic records, J. Geophys. Res. Atmos., 115, 1–27, https://doi.org/10.1029/2009JD013255, 2010.

Rodriguez-Caton, M., Morales, M. S., Rao, M. P., Nixon, T., Vuille, M., Rivera, J. A., Oelkers, R., Christie, D. A., Varuolo-Clarke, A. M., Ferrero, M. E., Magney, T., Daux, V., Villalba, R., and Andreu-Hayles, L.: A 300-year tree-ring δ18O-based precipitation reconstruction for the South American Altiplano highlights decadal hydroclimate teleconnections, Commun. Earth Environ., 5, 1–13, https://doi.org/10.1038/s43247-024-01385-9, 2024.

Rozanski, K., Sonntag, C., and Munnich, K. O.: Factors controlling stable isotope composition of European precipitation., Tellus, 34, 142–150, https://doi.org/10.3402/tellusa.v34i2.10796, 1982.

Rozanski, K., Araguãs-Araguãs, L., and Gonfiantini, R.: Relation between long-term trends of oxygen-18 isotope composition of precipitation and climate, Science, 258, 981–985, https://doi.org/10.1126/science.258.5084.981, 1992.

Schöne, B. R., Meret, A. E., Baier, S. M., Fiebig, J., Esper, J., Mcdonnell, J., and Pfister, L.: Freshwater pearl mussels from northern Sweden serve as long-term, high-resolution stream water isotope recorders, Hydrol. Earth Syst. Sci., 24, 673–696, https://doi.org/10.5194/hess-24-673-2020, 2020.

https://doi.org/10.5194/egusphere-2024-4169
Preprint. Discussion started: 17 February 2025

Slater, L. J. and Wilby, R. L.: Measuring the changing pulse of rivers, Science, 357, 552, https://doi.org/10.1126/science.aao2441, 2017.

Sodemann, H. and Zubler, E.: Seasonal and inter-annual variability of the moisture sources for alpine precipitation during 1995-2002, Int. J. Climatol., 30, 947–961, https://doi.org/10.1002/joc.1932, 2010.

Stumpp, C., Klaus, J., and Stichler, W.: Analysis of long-term stable isotopic composition in German precipitation, J. Hydrol., 517, 351–361, https://doi.org/10.1016/j.jhydrol.2014.05.034, 2014.

Sturm, C., Zhang, Q., and Noone, D.: An introduction to stable water isotopes in climate models: Benefits of forward proxy modelling for paleoclimatology, Clim. Past, 6, 115–129, https://doi.org/10.5194/cp-6-115-2010, 2010.

Urhausen, S., Brienen, S., Kapala, A., and Simmer, C.: Climatic conditions and their impact on viticulture in the Upper Moselle region, Clim. Change, 109, 349–373, https://doi.org/10.1007/s10584-011-0059-z, 2011.

Vodila, G., Palcsu, L., Futó, I., and Szántó, Z.: A 9-year record of stable isotope ratios of precipitation in Eastern Hungary: Implications on isotope hydrology and regional palaeoclimatology, J. Hydrol., 400, 144–153, https://doi.org/10.1016/j.jhydrol.2011.01.030, 2011.

Werner, M., Haese, B., Xu, X., Zhang, X., Butzin, M., and Lohmann, G.: Glacial-interglacial changes in H218O, HDO and deuterium excess-results from the fully coupled ECHAM5/MPI-OM Earth system model, Geosci. Model Dev., 9, 647–670, https://doi.org/10.5194/gmd-9-647-2016, 2016.